文章编号：1001－9014(2015)06－0647－07
DOI:10.11972/j.issn.1001－9014.2015.06.002

Noise analysis and structural optimal design of diode microbolometer uncooled IRFPAs

ZHU Hui-Hui[1,2], FENG Fei[1*], WANG Yue-Lin[1], LI Xin-Xin[1]

(1. State Key Laboratory of Transducer Technology, Shanghai Institute of Microsystem and Information Technology, Chinese Academy of Sciences, Shanghai 200050, China;
2. University of Chinese Academy of Sciences, Beijing 100049, China)

Abstract: The diode microbolometer uncooled IRFPAs (infrared focal plane arrays, IRFPAs) have shown broad prospects in recent years. The performance of the IRFPAs is limited by sources of noise from the detector itself which must be further studied and decreased to achieve better performance. This paper outlines sources of noise from the detector, quantifies the RMS (root-mean-square, RMS) noise voltages from different noise sources, discusses their implications and finally obtains performance limits of the diode microbolometer IRFPA. Moreover, the optimum structural parameters are also studied. The theoretical computation results show that the temperature fluctuation noise-limited NETD (noise-equivalent temperature difference, NETD) of the detector is 2.36mK with a corresponding radiation-limited conductance of 2.06 nW/K. In addition, the optimum NETD of 46.5 mK can be obtained when the detector operates in the forward bias current of 33 μA and the ratio of temperature sensing area is 54% in a 25 μm×25 μm micromachined structure.

Key words: infrared focal plane array (IRFPA), diode microbolometer, noise-equivalent temperature difference (NETD)
PACS: 07.57.Kp

二极管型红外焦平面阵列的噪声分析及结构优化设计

朱慧慧[1,2], 冯 飞[1*], 王跃林[1], 李昕欣[1]

(1. 中国科学院上海微系统与信息技术研究所 传感技术联合国家重点实验室,上海 200050;
2. 中国科学院大学,北京 100049)

摘要:二极管非制冷红外焦平面阵列(IRFPA)探测器具有广阔的前景,然而它的性能受噪声源的制约,为了得到高性能的探测器,必须研究噪声源并减小其影响.概述了探测器噪声源,量化并研究了不同噪声对探测器的影响,最后得到了二极管IRFPA的性能极限,此外,计算得到了最优的结构参数.理论研究表明温度起伏噪声对应的最小噪声等效温差(NETD)为2.36 mK,此时探测器热导为辐射热导,其值为2.06 nW/K.当单元尺寸为25 μm×25 μm的探测器的正向偏置电流为33 μA,占空比为54%时可得到最优NETD为46.5 mK.

关 键 词:非制冷红外焦平面阵列;二极管;噪声等效温差

中图分类号:TN215 **文献标识码**:A

Introduction

Nowadays, uncooled bolometer IRFPAs have become a good choice for low-cost infrared detector systems used in both civil and military applications such as medicine, firefighting, aircrafts, security and surveillance. Among all uncooled bolometer IRFPAs[1], the most common sensing materials or components in use are vanadium

Received date: 2014-10-20, **revised date**: 2015-09-30 **收稿日期**:2014-10-20, **修回日期**:2015-09-30
Foundation items:Supported by National Natural Science Foundation of China(61172151,60876081), National High Technology Research and Development Program of China (863 Program)(2009AA04Z317), and Science and Technology Commission of Shanghai Municipality, (14DZ1105102)
Biography:Zhu Hui-Hui(1990-), female, Jiangsu Province, China. Master degree candidate. Research area focuses on uncooled infrared detector. E-mail: zhuhuihui@mail.sim.ac.cn
* **Corresponding author**:E-mail:fengfei507@mail.sim.ac.cn

oxide (VO_x)[2-4], amorphous silicon (α-Si)[5-7], SiC/Al bi-material micro-cantilever[8-9] and silicon diodes[10-12].

Many scientific research institutions interested in the diode microbolometer uncooled IRFPAs working with different technologies have produced a variety of creative research results recently[10-11]. Till now, Mitsubishi Electric Corporation has developed a 2-million-pixel SOI diode uncooled IRFPA with a 15 μm pixel pitch, and its NETD is 65 mK[12]. Comparison of several different temperature sensing materials or components of bolometer IRFPAs is made in Table 1. After comparison and analysis, a conclusion is drawn that the PN junction diode has some advantages such as occupying small area, having low 1/f noise, being of great consistency and being compatible with conventional silicon IC process. Thus it is suitable for fabricating high-performance uncooled thermal detectors. Many scholars have done a lot of research works in performance limits of VO_x and α-Si microbolometer detectors[13-14], while so far nobody does systematic research and detailed analysis of diode microbolometer detectors. The paper focuses mainly on studying noise analysis, performance limits and structural design of diode microbolometer uncooled IRFPAs. This is significant for researchers to have a deeper understanding of the diode microbolometer detector in order to make further progress in the future.

Table 1 Comparison of different temperature sensing materialsor components of bolometer IRFPAs[1]

表 1 基于不同敏感材料或元器件的电阻型红外焦平面阵列性能的比较[1]

Sensing materials or components	Advantages	Disadvantages
VO_x	Low 1/f noise, appropriate electrical resistivity	Not compatible with conventional silicon IC process
α-Si	Compatible with conventional silicon IC process	High 1/f noise
SiC/Al bi-material micro-cantilever	Good NETD in theory, silicon IC compatibility	Low yield, difficult manufacture process
PN junction diode (monocrystallinesilicon)	low 1/f noise, smaller size, compatible with conventional silicon IC process	Low voltage-temperature coefficient(about 0.2%/K)

1 Theory and structure of the PN junction diode

The pixel structure sketch of a diode microbolometer uncooled IRFPA is shown in Fig. 1 alongside a corresponding section figure explaining the structure in detail. Figure 2 is a SEM (scanning electron micrograph, SEM) graph of a pixel of the diode uncooled IRFPA manufactured by our laboratory. The diode microbolometer uncooled IRFPA uses PN junction diodes as temperature sensors and each pixel consists of several diodes in series suspended above a cavity by two thin narrow supporting legs fabricated through a micromachining process. In addition, it is notable that the thermal conductance of the IRFPA depends on the structural parameters of the supporting legs. Furthermore, a freestanding infrared absorber made by surface micromachining process is sometimes also needed to obtain a high fill factor. It is worth noting that the array is monolithic and produced using mature Si-LSI process and micromachining techniques. All of these make sure that the IRFPAs can be fabricated at low cost and in high yield.

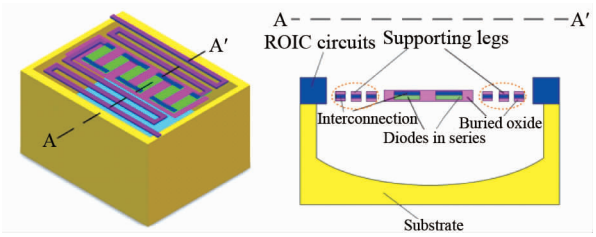

Fig. 1 3D diagram and section graph of a pixel of a diode microbolometer uncooled IRFPA

图 1 二极管非制冷红外焦平面阵列单元三维结构图和截面图

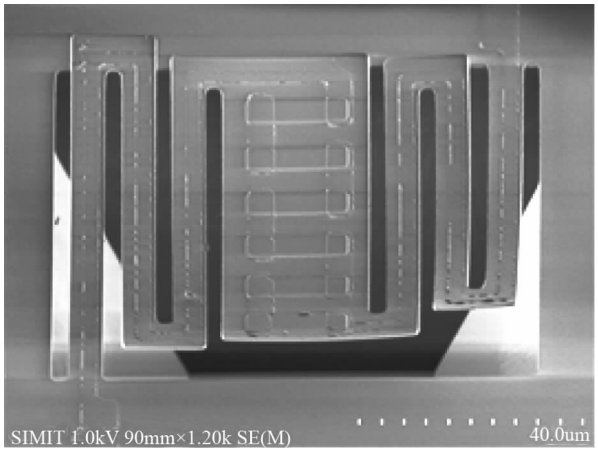

Fig. 2 SEM graph of a pixel of a diode microbolometer uncooled IRFPA

图 2 二极管非制冷红外焦平面阵列单元 SEM 图

The diode microbolometer uncooled IRFPA using PN junction diodes as infrared sensors utilizes the diode's voltage-temperature characteristics to realize infrared imaging. The forward bias current of an ideal diode is given by[15]:

$$I_f = I_s\left(e^{\frac{qV_f}{kT}} - 1\right), \quad (1)$$

where I_s is the reverse saturation current, I_f is the forward current flowing through the diode, V_f is the output voltage across the terminals of the diode, q is the absolute value of electron charge, k is Boltzmann's constant, and T is absolute temperature. The reverse saturation current I_s can be expressed as[15]:

$$I_s \approx T^{(3+\gamma/2)} e^{-\frac{qV_g}{kT}}, \quad (2)$$

where V_g is the voltage correlated with the energy gap of the semiconductor material to fabricate the PN junction diode, and γ is a constant. Supposed $T = 300\text{K}$, $kT/q = 26$ mV, when the forward bias voltage $V_f \gg 26$ mV, Eq. 1 can be simplified as:

$$I_f \approx T^{(3+\gamma/2)} e^{-\frac{q(V_f - V_g)}{kT}}. \quad (3)$$

So V_f can be expressed by:

$$V_f = \left(\frac{k}{q}\ln I_f\right)T + V_g - \frac{3+\gamma/2}{q}kT\ln T \quad . \quad (4)$$

V_f can be divided into two parts, $V_f = V_1 + V_2$, where $V_1 = (k\ln I_f/q)T + V_g$, $V_2 = -(3+\gamma/2)kT\ln T/q$. When the forward bias current of a PN junction diode keeps constant, V_1 is linear to the temperature. Analyzing V_2, $d(T\ln T)/dT = 1 + \ln T$, if $T > 1/e$, $d(T\ln T)/dT > 0$, $T\ln T$ monotonically increases as temperature increases; $d^2(T\ln T)/dT^2 = 1/T$, if T is large enough, $\lim_{T\to\infty} d^2(T\ln T)/dT^2 = 0$, under this condition, V_2 is linear to the temperature.

If I_f is small enough, $|\ln I_f| >> (3+\gamma/2)\ln T$, that is, $|V_1| >> |V_2|$, $V_f \approx V_1$. An approximate relationship is obtained that V_f is linear to the temperature when the forward bias current is a constant and small enoughas shown in Fig. 3.

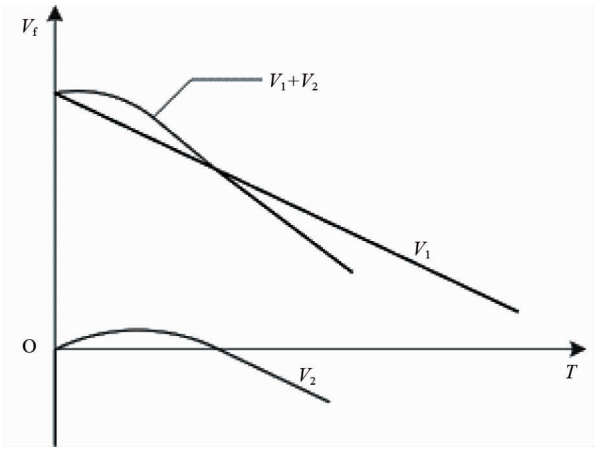

Fig. 3　Dependence of forward bias voltage on temperature
图 3　正向偏置电压与温度的关系

Under the condition of a constant forward bias current, the diode's voltage-temperature relation can be expressed as:

$$\left.\frac{dV_f}{dT}\right|_{\text{const } I_f} = -\frac{[qV_g + (3+\gamma/2)kT] - qV_f}{qT} \quad . \quad (5)$$

As to a typical silicon PN junction diodeoperating at the voltage, 0.7 V, it has a temperature sensitivity of about 2 mV/K at room temperature[1].

2　Noise analysis

Noise in a diode microbolometer system generally comes from three sources: the detector itself, the electronics (ROIC and image processing electronics), and other system sources. In general, performance is mainly limited by noise in the detector itself among all of these sources of noise[13]. This paper focuses on discussing noise of the detector itself.

There are four major sources of noise originating in the diode microbolometer detector. These include temperature-fluctuation noise, Johnson noise, shot noise and $1/f$ noise.

2.1　Temperature fluctuation noise

Temperature fluctuation noise, arising from random exchange of heat between the microbolometer and its environment, results in random fluctuations in the detector temperature. The mean square temperature fluctuation noise, $\overline{v_{TF}^2}$, from the random exchange of the pixel and its surroundings is given by[16]:

$$\overline{v_{TF}^2} = 4kG_{th}T^2R^2(\omega)\Delta f_{th} \quad , \quad (6)$$

where G_{th} is the thermal conductance, $R(\omega)$ is the responsitivity of the detector, ω is angular frequency, and Δf_{th} is the thermal bandwidth. The temperature fluctuation noise-limited detectivity $D^*_{0\text{-}TF}$, is shown as[17]:

$$D^*_{0\text{-}TF} = \frac{\eta}{2T}\left[\frac{A_D}{kG_{th}}\right]^{1/2} \quad , \quad (7)$$

where η is the absorption coefficient, and A_D is the detector area.

The temperature fluctuation noise-limited NETD is proportional to $G_{th}^{1/2}$ as shown below[17]:

$$\text{NETD}_{0\text{-}TF} = \frac{8F^2T[kG_{th}\Delta f_{th}]^{1/2}}{\eta\tau_0 A_D(\Delta P/\Delta T)_{\lambda_1-\lambda_2}} \quad , \quad (8)$$

where F is the optical f/number, τ_0 is the transmittance of the optics, and $(\Delta P/\Delta T)_{\lambda_1-\lambda_2}$ is the blackbody differential emittance. The temperature fluctuation noise existing in thermal detectors ultimately limits the minimum radiation energy that can be detected by the detector. Usually, it is the fundamental limit on the performance of thermal detectors.

2.2　The main sources of noise in a PN junction diode

The main sources of noise in a PN junction diode are Johnson noise, shot noise and $1/f$ noise. The forward bias voltage V_f is shown as[10]:

$$V_f = \frac{kT}{q}\ln\left(\frac{I_r}{I_s}\right) + I_f r_s \quad , \quad (9)$$

where r_s is the resistance of neutral semiconductor region. From Eq. 9, the differential resistance is given by:

$$\frac{dV_f}{dI_f} = \frac{kT}{qI_f} + r_s \quad . \quad (10)$$

Referring to Ref. [18], the complete diode small-signal equivalent circuit with noise sources is shown in Fig. 4. Since r_s is a physical resistor, it exhibits Johnson noise. In addition, $1/f$ noise combined with shot noise can be equivalent to a current generator, $\overline{i^2}$, in shunt with $r_d = kT/qI_f$, as shown below:

$$\overline{v_{jn}^2} = 4kTr_s\Delta f \quad , \quad (11)$$

$$\overline{i^2} = 2qI_f\Delta f + k_1\frac{I_f^b}{f^a}\Delta f \quad , \quad (12)$$

where $\overline{v_{jn}^2}$ is the mean square Johnson noise voltage, $\overline{i^2}$ is the mean square current noise (shot noise, $\overline{v_{sn}^2} = 2qI_f\Delta f$, and $1/f$ noise, $\overline{v_{fn}^2} = k_1\frac{I_f^b}{f^a}\Delta f$), Δf is electrical bandwidth, k_1 is the flicker noise coefficient, a is a constant of about unity, and b is a constant in the range of 0.5 to 2[18].

Combining Eqs. 11 and 12, the mean square shot noise and $1/f$ noise voltages are shown below:

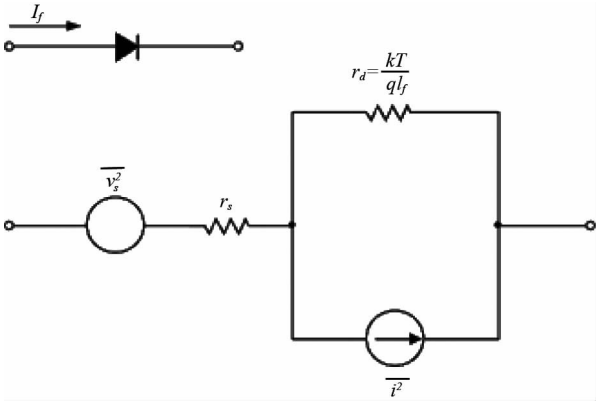

Fig. 4 Complete diode small-signal equivalent circuit with noise sources

图4 二极管噪声等效模型

$$\overline{v_{sn}^2} = \frac{2k^2T^2\Delta f}{qI_f} \quad , \quad (13)$$

$$\overline{v_{fn}^2} = k_1\frac{k^2T^2I_f^{b-2}}{q^2f^a}\Delta f \quad . \quad (14)$$

Assuming that the output noise voltage is v_N, than the responsivity[16] of the noise is given by:

$$R = \frac{v_N}{P_0} = \frac{\eta}{G_{th}}\left(\frac{dV}{dT}\right)\frac{1}{\sqrt{1+\omega^2\tau^2}} \quad , \quad (15)$$

where P_0 is power amplitude of radiation, dV/dT is voltage-temperature coefficient of the PN junction, and τ is the thermal response time.

The noise-equivalent power (NEP)[16] is given by:

$$NEP = \frac{v_N}{R} = \frac{G_{th}v_N\sqrt{1+\omega^2\tau^2}}{\eta(dV/dT)} \quad . \quad (16)$$

The defining equation for the detectivity(D^*)[16] is given by:

$$D^* = \frac{\sqrt{A\Delta f}}{NEP} = \frac{\eta}{G_{th}v_N}\left(\frac{dV}{dT}\right)\sqrt{\frac{A_D\Delta f}{1+\omega^2\tau^2}} \quad , \quad (17)$$

then the NETD[16] is given below:

$$NETD = \frac{4F^2\sqrt{\Delta f}}{\tau_0\sqrt{A_D}(\Delta P/\Delta T)_{\lambda_1-\lambda_2}}\cdot\frac{1}{D^*} = \frac{4F^2G_{th}v_N}{\eta\tau_0A_D(dV/dT)(\Delta P/\Delta T)_{\lambda_1-\lambda_2}}\sqrt{1+\omega^2\tau^2} \quad . \quad (18)$$

Combining Eqs. 11, 13-14 and 17, the detectivity limited by Johnson noise, shot noise and $1/f$ noise are shown below, respectively:

$$D^*_{0\text{-jn}} = \frac{\eta}{G_{th}}\left(\frac{dV}{dT}\right)\left(\frac{A_D}{4kTr_s(1+\omega^2\tau^2)}\right)^{1/2} \quad , \quad (19)$$

$$D^*_{0\text{-sn}} = \frac{\eta}{kTG_{th}}\left(\frac{dV}{dT}\right)\left(\frac{qI_fA_D}{2(1+\omega^2\tau^2)}\right)^{1/2} \quad , \quad (20)$$

$$D^*_{0\text{-fn}} = \frac{\eta}{G_{th}v_{fn}}\left(\frac{dV}{dT}\right)\left(\frac{A_D\Delta f}{1+\omega^2\tau^2}\right)^{1/2} \quad , \quad (21)$$

where v_{fn} is the RMS voltage of flicker noise.

Combing Eqs. 11, 13-14 and 18, the NETD limited by Johnson noise, shot noise and $1/f$ noise are shown below:

$$NETD_{0\text{-}jn} = \frac{8F^2G_{th}}{\eta\tau_0A_D(dV/dT)(\Delta P/\Delta T)_{\lambda_1-\lambda_2}[(kTr_s\Delta f)(1+\omega^2\tau^2)]^{1/2}} \quad , \quad (22)$$

$$NETD_{0\text{-sn}} = \frac{4F^2kTG_{th}}{\eta\tau_0A_D(dV/dT)(\Delta P/\Delta T)_{\lambda_1-\lambda_2}\left[\frac{2\Delta f(1+\omega^2\tau^2)}{qI_f}\right]^{1/2}} \quad , \quad (23)$$

$$NETD_{0\text{-fn}} = \frac{4F^2G_{th}v_{fn}}{\eta\tau_0A_D(dV/dT)(\Delta P/\Delta T)_{\lambda_1-\lambda_2}[1+\omega^2\tau^2)]^{1/2}} \quad . \quad (24)$$

By studying Eqs. 7, 19, 20 and 21 or Eqs. 8, 22-24, all the internal and external factors affecting NETD can be listed. The external factors are the forward bias operating current, the optical f/number, and the internal factors include the thermal conductance, the RMS voltage of different noise, the area of the detector, and the voltage-temperature coefficient of the PN junction diode. All of these factors should be taken into considerations when designing a good performance diode microbolometer uncooled IRFPA.

3 Performance analysis and parameter optimization design

This section mainly focuses on studying and analyzing factors that affect the performance of the diode microbolometer infrared detector. After calculation, the optimum structure parameters and forward bias current were obtained, in addition, the approaches to reducing impact of $1/f$ noise on performance of the detector were also put forward and discussed.

3.1 Limiting NETD

In Fig. 5, the pixel size of the IR detector is 25 μm ×25 μm, the ratio of temperature sensing area is 24% of the whole area, and the ratio of etching area is 29%. The width of the beam is 0.5μm and the length of one side of the supporting legs is 60 μm. When radiation exchange dominates, G_{rad} is with respect to the temperature of the Stefan-Boltzmann expression[17]:

$$G_{rad} = 4A_{eff}\varepsilon\sigma T^3 \quad , \quad (25)$$

where A_{eff} is the detector effective area, ε is the emissivity (here $\varepsilon=0.8$), and σ is the Stefan-Boltzmann constant. After calculation, G_{rad} is 2.06 nW/K for the pixel. From Eq. 6, the detector has a minimum NETD of 2.36 mK when the radiation-limited conductance is 2.06 nW/K. In order to achieve the thermal conductance approaching the radiation-limited conductance, thermal conductance coming from air and supporting legs should be decreased. As heat can transfer through the surrounding atmosphere by conduction and convection, an evacuated package to decrease the thermal conductance originating from the air is crucial to the IRFPA. In addition, as heat can flow from the sensing area via the supporting legs to the substrate, the structural parameters of the legs should be designed carefully to minimize thermal conductance of the supporting legs.

3.2 Dependence of NETD on forward bias operating current and structure parameters

The thermal conductance of the dector is given

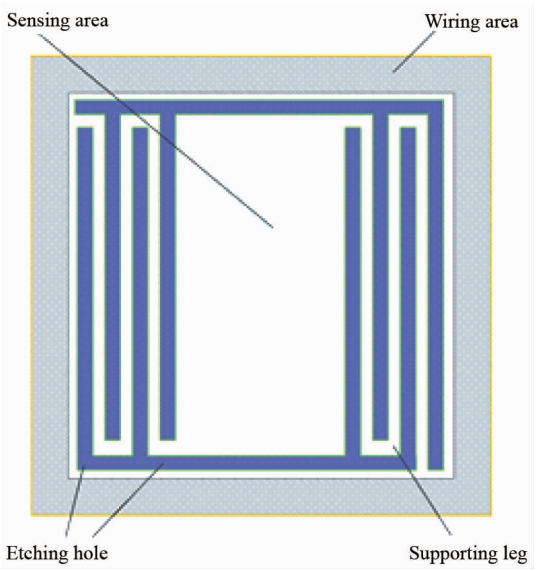

Fig. 5　Top view of one pixel of the IR detector
图 5　红外探测器单元俯视图

by[19]:

$$G_{\mathrm{th}} = G_{\mathrm{rad}} + G_{\mathrm{leg}} = 4A_{\mathrm{eff}}\varepsilon\sigma T^3 + \sum_i \frac{\lambda_i \omega_i d_i}{l_i}, \quad (26)$$

where G_{leg} is the thermal conductance of the supporting legs, λ_i, ω_i, d_i, l_i are the width, thermal conductivity, thickness, and length of specific films, respectively.

Supposed $k_1 = 1\mathrm{e}\text{-}12$[20], $a = 1$, $b = 1.5$[10], $I_s = 3\mathrm{E}\text{-}19$ A[10], $r_s = 1.5$ kΩ[10], $\Delta f_{\mathrm{th}} = 30$ Hz, $\eta = 0.8$, and $\tau_0 = 1$, the electrical frequency is in the range of 0.000 1 Hz[17] to 8 000 Hz[13] and the legs is folded by n times as the way shown in Fig. 5. According to the process conditions, the width of the supporting legs is 0.5 μm, and the thickness is 0.4 μm. In addition, the pixel size is 25 μm × 25 μm in order to obtain larger arrays. After optimizing both forward bias current and length of the legs by changing parameter n, the total NETD of six PN junctions in series of diode microbolometer uncooled IRFPAs can be calculated through the above Eqs. 8, and 22-24. As shown in Fig. 6, there exists the minimum NETD of 46.5 mK when the forward bias current is 33 μA and the legs are folded by 5 times.

3.2.1　Dependence of NETD on structure parameters

As the effects of forward bias current and structure parameters on NETD are independent, they can be discussed respectively. Supposing the forward bias operating current is 33 μA, the optimum NETD is obtained when the legs are folded by 5 times. As shown in Fig. 7, when n is less than 5, the total NETD is improved because the decreased thermal conductance plays the leading role. When n is more than 5, The NETD increases for that the reduction of absorption area takes the dominant place. So the optimal value of $n = 5$ can be achieved and the corresponding NETD is 46.5 mK. When $n = 5$, the length of the supporting legs is 123 μm, the ratio of the temperature sensing area is 54%, and the total thermal conductance is 14 nW/K. The optimal structural parameters are listed in Table 2.

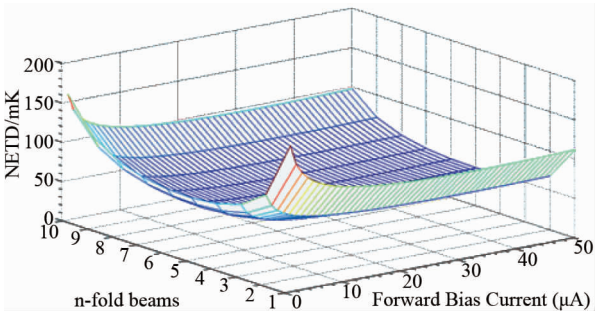

Fig. 6　Caculated NETD of six PN junctions in series versus forward bias current and n
图 6　NETD 与正向偏置电流以及梁折叠次数 n 的关系

Table 2　Optimal structural parameters of the diode microbolometer IRFPA
表 2　二极管型红外焦平面阵列的结构优化参数

Pixel Size	25 μm × 25 μm
Width of the supporting legs	0.5 μm
Thickness of the supporting legs	0.4 μm
Length of the supporting legs	123 μm
Ratio of temperature sensing area	54%
Thermal conductance	14 nW/K

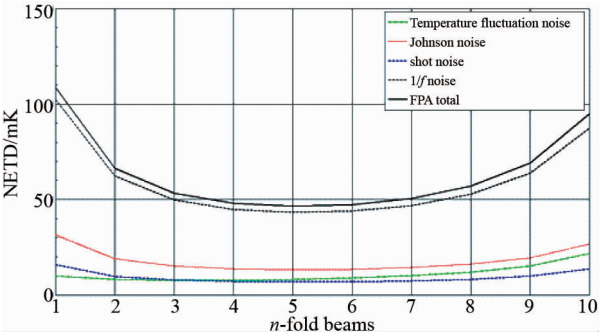

Fig. 7　Caculated NETD of six PN junctions in series versus n ($@\ I_f = 33$ μA)
图 7　NETD 与梁折叠次数 n 的关系

4.2.2　Dependence of NETD on forward bias operating current

As shown in Fig. 8, the total FPA noise decreases when the forward bias current increases. As shown in Fig. 9, when the forward bias current increases up to 20 μA, the total NETD is improved because the total RMS noise, which sharply decreases, plays the leading role. However, the NETD remains almost constant over this value because the total RMS noise changes slowly when the forward bias current is in the range of 20 μA to 40 μA. The NETD gradually increases when the forward bias current exceeds 40 μA for that the reduction of the voltage-temperature coefficient takes the dominant place. Through analyzing and calculating, the optimum forward bias current of 33 μA can be adopted where the minimum NETD of 46.5 mK is obtained.

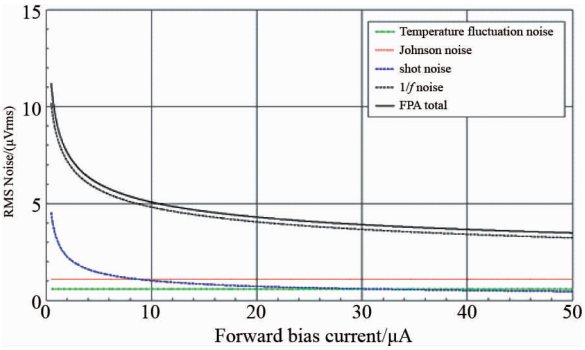

Fig. 8 Caculated RMS noise of six PN junctions in series versus forward bias current (@ $n=5$)
图 8 平方根噪声值与正向偏置电流的关系

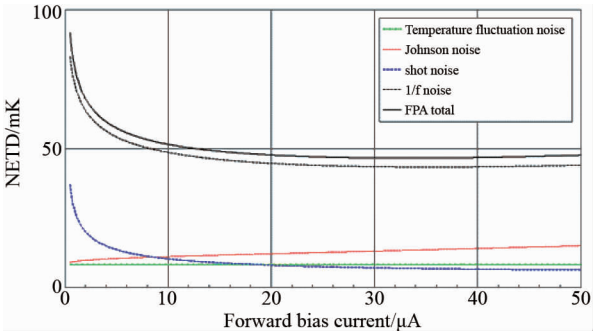

Fig. 9 Caculated NETD of six PN junctions in series versus forward bias current (@ $n=5$)
图 9 NETD 与正向偏置电流的关系

3.3 Performance improvement trade offs

After analysis and calculation, a conclusion can be drawn that $1/f$ noise plays the dominant role in performance of the diode microbolometer uncooled IRFPA. To improve performance of the detector, the impact of $1/f$ noise must be reduced in the detector. By studying Eq. 24, there are at least three methods that can reduce impact of $1/f$ noise on the total FPA noise:

(1) reducing the thermal conductance of the supporting legs;

(2) reducing the inherent $1/f$ noise of the PN junction diode; and

(3) increasing the forward bias current (within 33 μA).

Thermal time constant is also an important factor of the detector which should be taken into considerations when improving the performance of the IRFPA. It is defined as[17]:

$$\tau = \frac{C}{G_{\text{th}}} \quad , \quad (27)$$

where C is the heat capacity of the bridge.

If C is a constant, than $\tau \propto 1/G_{\text{th}}$. In addition, seeing Fig. 9, the total NETD is dominated by $\text{NETD}_{0\text{-fn}}$ depended on $1/f$ noise which is proportional to G_{th}, that is, $\text{NETD} \approx \text{NETD}_{0\text{-fn}} \propto G_{\text{th}}$. All of these show that the total NETD of the detector is roughly inversely proportional to its thermal time constant:

$$\text{NETD} \propto \frac{1}{\tau} \quad . \quad (28)$$

There exists a trade off for improving the detector sensitivity when changing a parameter of the detector for that it may have a negative impact on the thermal time constant. If reducing the thermal conductance of the supporting legs, the NETD reduces while the thermal time constant increases. If reducing the inherent $1/f$ noise of the PN junction diode, the NETDis improved, meanwhile, the thermal time constant keeps unchanged. If increasing the forward bias current (within 33 μA), the reduction of total RMS noise plays the leading role, and the reduction of the voltage-temprature coefficient takes the secondary place, then the NETD decreases, and the thermal time constant remains the same under this condition.

4 Conclusions

There are four major sources of noise existing in the diode microbolometer detector: temperature-fluctuation noise, Johnson noise, shot noise and $1/f$ noise, among which $1/f$ noise takes the dominant place while temperature-fluctuation noise primarily limits the minimum attainable NETD. The theoretical computation results show that the temperature fluctuation noise-limited NETD of the detector is 2.36 mK with a corresponding radiation-limited conductance of 2.06 nW/K. In addition, the minimum NETD of 46.5 mK can be obtained when the forward bias current is 33 μA and the legs are folded by 5 times. After comparison between the designed and actual detector[10] in Table 3, the performance of the designed detector still approaches the actual detector without IR absorber and reflector.

Table 3 Summary of the performance of the designed diode microbolometer IRFPA
表 3 二极管型红外焦平面阵列探测器的性能参数

	Designed detector	Actual detector
Pixel Size	25 μm×25 μm	25 μm×25 μm
Structure Design	No IR Absorber and Reflector	Including IR Absorber and Reflector
Ratio of IR Absorbing Structure	54%	90%
Thermal Conductance	14 nW/K	16 nW/K
NETD (f/1.0)	46.5 mK	40 mK
Thermal Time Constant	21 ms	24 ms

In order to fabricate a high performance detector, there are at least three ways: reducing the thermal conductance, which will reduce the temperature fluctuation noise-limited NETD and the total NETD; reducing the $1/f$ noise of the diode, which will reduce the total NETD; increasing the forward bias current within 33 μA, which will also reduce the total NETD. The first approach has a trade off between improving the NETD of the detector and increasing the thermal time constant. The other two ways have no impact on the thermal time constant. In conclusion, all the factors should be taken into account when improving the sensitivity of the diode microbolometer uncooled IRFPAs.

Acknowledgements

This research was partly supported by projects of Natural Science Foundation of China, No. 61172151 and No. 60876081, the National High Technology Research and Development Program of China (863 Program), No. 2009AA04Z317, and the Science and Technology Commission of Shanghai Municipality, China, No. 14DZ1105102.

References

[1] Niklaus F, Vieider C, Jakobsen H. MEMS-Based Uncooled Infrared Bolometer Arrays - A Review [J]. *Proc. SPIE*, *MEMS/MOEMS Technologies and Applications III*, 2007, **6836**: 68360D-1-15.

[2] Chen C, Yi X, Zhang J, *et al*. Micromachined uncooled IR bolometer linear array using VO2 thin films[J]. *International Journal of Infrared and Millimeter Waves*, 2001, **22**(1): 53.

[3] Wood R A. Uncooled thermal imaging with monolithic silicon focal planes [J]. *Proc. SPIE*, *Infrared Technology XIX*, 1993, **2020**: 322-329.

[4] Li C, Skidmore G D, Han C J. Uncooled VO_x infrared sensor development and application [J]. *Proc. SPIE*, *Infrared Technology and Applications XXXVII*, 2011, **8012**: 80121N-1-8.

[5] Heredia A, De La Hidalga F J, Torres A, *et al*. Low temperature electrical properties of a boron-doped amorphous silicon bolometer [J]. *Proc. The Electrochemical Society* 2003, **204**: Abs. 881.

[6] Tissot J L, Rothan F, Vedel C, *et al*. LETI/LIR's amorphous silicon uncooled microbolometer development [J]. *Proc. SPIE*, *Infrared Detectors and Focal Plane Arrays V*, 1998, **3379**: 139-144.

[7] Tissot J L, Robert P, Durand A, *et al*. Status of uncooled infrared detector technology at ULIS, France [J]. *Defence Science Journal*, 2013, **63**(6): 545.

[8] Amantea R, M. Knoedler C, Pantuso F P, *et al*. An Uncooled IR imager with 5mK NETD. *Proceedings of SPIE Vol.* 3061, *Orlando*, April, 1997: 210-222.

[9] Hunter S R, Amantea R A, Goodman L A, *et al*. High Sensitivity Uncooled Microcantilever Infrared Imaging Arrays [J]. *Proc. SPIE*, *Infrared Technology and Applications XXIX*, 2003, **5074**: 469-480.

[10] [10] Ueno M, Kosasayama Y, Kimata M, *et al*. 640x480 pixel uncooled infrared FPA with SOI diode detectors [J]. *Proc. SPIE*, *Infrared Technology and Applications XXXI*, 2005, **5783**: 567-577.

[11] Kwon H, Suzuki K, Ishii K, *et al*. A SOI-based CMOS-MEMS IR image sensor with partially released reference pixels [J]. *Journal of micromechanics and microengineering*, 2011, **21**: 025028-6.

[12] Fujisawa D, Maegawa T, Ohta Y, *et al*. 2-million-pixel SOI diode uncooled IRFPA with 15 μm pixel pitch [J]. *Proc. SPIE*, *Infrared Technology and Applications XXXVIII*, 2012, **8353**: 83531G-1-13.

[13] Kohin M, Butler N R. Performance limits of uncooled VO_x microbolometerfocal plane arrays [J]. *Proc. SPIE*, *Infrared Technology and Applications XXX*, 2004, **5406**: 447-453.

[14] Sun L J, Chang B K, Zhang J J, *et al*. Thermal and electrical performance of α-Si microbolometer focal plane arrays [J]. *Proc. SPIE*, *International Conference on Smart Materials and Nanotechnology in Engineering*, 2007, **6423**: 64232D-1-6.

[15] Sze S M, Ng K K. *Physics of Semiconductor Devices*. [M]. Hoboken, USA: Wiley, third ed, 2007.

[16] Oloomi H M, Alam M S, Rana M M. Noise performance evaluation of uncooled infrared detectors [J]. *IEEE sensors journal*, 2011, **11**(4): 971.

[17] Kruse P W, Skatrud T W. *Uncooled infrared imaging arrays and systems*[M]. Salt Lake City, USA: Academic Press, 1997.

[18] Gray P R, Hurst P J, Lewis S H, *et al*. *Analysis and design of analog integrated circuits*. [M]. Hoboken, USA: Wiley, fifth ed., 2009.

[19] Jiang W J, Ou W, Minga J, *et al*. Design and analysis of a high fill-factor SOI diode uncooled infrared focal plane array [J]. *J. Micromech. Microeng.*, 2013, **23**: 065004-5.

[20] Ahmed M, Butler D P, Celik-Butler Z. The flicker noise in amorphous silicon based temperature sensors in flexible substrates [J]. *IEEE*, *21st International Conference on noise and fluctuations*, 2011: 154-157.